CHAPTER 2: BACKGROUND

In this chapter the background of nonlinear dynamics and electrochemistry that is necessary to understand the results presented in chapters 4-8 is summarized. First, the basic concepts from the theory of nonlinear dynamics are introduced (section 2.1). After presenting the main features of systems displaying temporal symmetry breaking, more precisely bistability and oscillations, a few remarks on the behavior of a population of individual oscillators coupled by diffusion are made. Section 2.2 deals with the interface between the fields of electrochemistry and nonlinear dynamics. Emphasis is put on introducing the jargon used in the thesis. In section 2.3 the different electrochemical systems studied are presented.

The chapter ends with a brief description of the method used to analyze and characterize the spatiotemporal patterns.

2.1 NONLINEAR DYNAMICS

2.1.1 BISTABILITY

Multistability is a widespread phenomenon and corresponds to the situation in which, under the same conditions, the system can exist in different stable steady states. *Bistability* refers to the situation in which two stable steady states coexist. Common to all systems displaying bistability is the presence of a self-enhancing process. In most cases the self-enhancement is due to an *autocatalysis*, i.e., an intermediate catalyses its own production. Thus, autocatalysis is the prominent mechanism responsible for the occurrence of a *positive feedback loop*.

Bistable dynamics can be explained with the help of Figure 2.1. In this figure, the variable x accounting for one property of the system is plotted as a function of a parameter or constraint μ. In this example, high x values correspond to an active state, whereas in the passive state the x values are low.

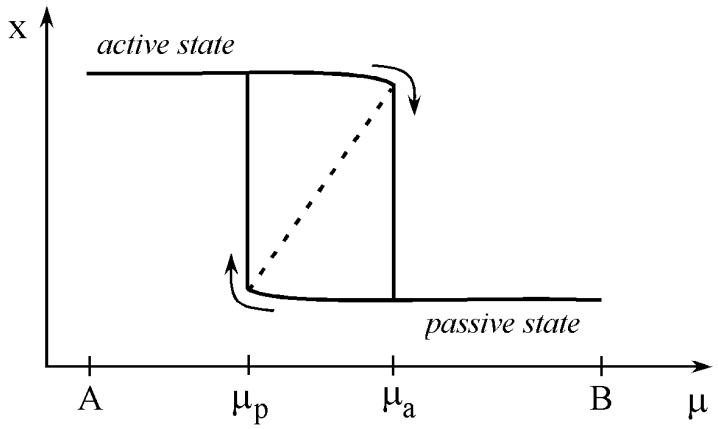

Figure 2.1: Variable x as a function of the control parameter μ, illustrating bistability between an active and a passive state in the range $\mu_p < \mu < \mu_a$.

As shown in Figure 2.1, between μ_a and μ_p, x can assume values corresponding to the active or the passive state depending on the direction in which μ has been varied. In fact,

when increasing μ from A, the active state is stable up to a critical value of μ_a. At this value a sharp transition from the active to the passive state is observed. On the other hand, when μ is decreased from B, the system stays in the passive state up to μ_p and then jumps back to the active branch. The dotted line connecting the borders of active and passive states represents an unstable state. It is not visited when sweeping μ, instead, a *hysteresis* loop is observed between μ_a and μ_p.

The points μ_a and μ_p are critical in a sense that at these points the dynamics of the system undergoes qualitative changes. Whenever the dynamics of a system experiences a qualitative change, a *bifurcation* is said to occur. In the case of the creation or annihilation of fixed points, as exemplified in Figure 2.1, at $\mu = \mu_a$ in the forward scan or $\mu = \mu_p$ along the backward scan, a *saddle-node bifurcation* is observed.

2.1.2 OSCILLATIONS

It was said in the previous section that bistable systems are characterized by the presence of a positive feedback loop. Addition of a second, negative, feedback loop that counteracts the positive loop can lead to oscillations. Positive and negative feedback loops are also referred to as *destabilizing* and *stabilizing* loops, respectively [54]. A system possessing such a combination of positive and negative feedback loops is called an activator-inhibitor system and may oscillate in a certain parameter range if the time scale of the inhibitor is slower than the one of the activator.

Figure 2.2 illustrates the situation in which a *limit cycle* is born when varying the parameter μ. Shown in this figure are the bifurcation diagram in terms of the variables x_1 and x_2 (plate (a)), and the phase space illustrating the stable focus ($\mu < 0$) and the limit cycle ($\mu > 0$) (plate (b)). Upon changing the parameter μ the stable focus becomes unstable when $\mu = 0$ and a stable limit cycle is born via a mechanism referred to as a *Hopf bifurcation*.

The case depicted in Figure 2.2 refers to the *supercritical* Hopf bifurcation and is characterized by a smooth or soft onset of stable oscillations whose amplitude grows proportionally to the square root of $\mu - \mu_c$ in the vicinity of the bifurcation point μ_c.

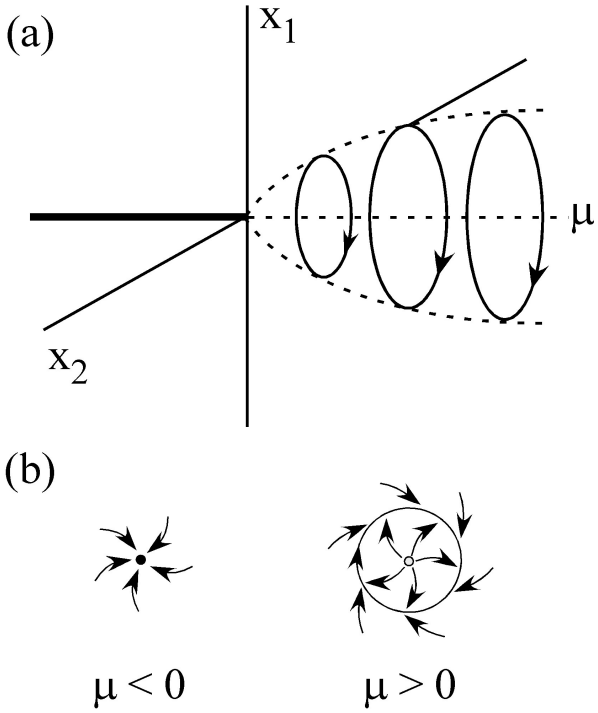

Figure 2.2: (a) Bifurcation diagram illustrating the Hopf bifurcation, and (b) the phase space corresponding to the stable focus (for $\mu < 0$) and the limit cycle ($\mu > 0$).

2.1.3 SPATIALLY EXTENDED SYSTEMS

A *point-like* system is defined as a system that lacks any spatial extension. In an *extended* or *distributed* oscillatory system, the system can be thought of as being composed of many individual oscillators[1]. Understanding the dynamical evolution or the collective behavior of these individual oscillators in an electrochemical environment as a function of different constraints is one of the main goals of this thesis. In this section the bridge connecting the point-like system to the extended system is presented. The starting point in building this bridge is to understand how these individual oscillators exchange information among each other, or, in other words, how they are *coupled*. Systems, in which several individual 'reacting' elements are coupled by diffusion are called *reaction-diffusion* (RD) systems and are considered as a paradigm for pattern formation (see, e.g., refs. [9, 30, 55] and references therein). Spatiotemporal patterns in RD systems result from the interaction of the

[1] Spatially extended systems might also behave as point-like systems if the different positions in space are coupled to each other so strongly that the system's dynamics is uniform in space. In a general situation, however, the spatial extension has to be taken into account.

homogeneous or reaction dynamics with the spatial transport processes. In mathematical terms, this class of systems is described by coupled partial differential equations. The evolution of variables, such as the concentration of reacting species, can be decomposed into the *reaction part*, which depends only locally on the value of the other variables and the *transport processes* that are induced by spatial variations in the variables and constitute a spatial coupling among different locations. Therefore, simple RD equations can formally be written as,

$$\frac{\partial c_i}{\partial t} = f_i\left(c_j, \mu_k\right) + D_i \nabla^2 c_i \qquad (2.1)$$

in which c_i are the variables, μ_k accounts for the parameters (or constraints) affecting the system's dynamics and can be externally controlled, the f_i are the nonlinear functions of the reaction part, and the D_i are the (constant) diffusion coefficients. The last term in equation (2.1) accounts for the transport process that couples the different locations in space with each other and provides the system's ability to exchange information between different parts. The way in which chemical reactions and diffusion cooperate in a symmetry breaking bifurcation can be intuitively understood as follows. The chemical kinetics, via its intrinsic feedback loops such as autocatalysis, may trigger a local 'runaway' phenomenon by amplifying the effect of small fluctuations. Diffusion, in turn, tends to spread the inhomogeneous distribution caused by the reaction. When its rate is comparable to the reaction rate, this homogenization might not be effective. Thus, a spatial pattern may form. The characteristic length of the pattern depends only on specific properties of the system, such as diffusion coefficients and reaction constants. For small systems, however, the diffusive 'stirring' is effective, the system takes on uniform states only, and behaves thus identically to the corresponding 'point-like system'.

Besides the diffusion coupling mentioned above, another type of interaction termed *global coupling* can exist if a local change of a variable is felt everywhere with the same strength independently of the distance with respect to the location of the perturbation. In this thesis situations play a role in which the global coupling shows up as an additive term. The equation describing RD systems in the presence of global additive coupling is given as,

$$\frac{\partial c_i}{\partial t} = f_i\left(c_j, \mu_k, \alpha\right) + D_i \nabla^2 c_i + \alpha\left(\langle c_i \rangle - c_i\right). \qquad (2.2)$$

Here, the squared brackets indicate the spatial average, the parameter α is the strength of the global coupling, and it may also enter the reaction part. If $\alpha > 0$, the global coupling acts towards synchronization, it is often referred to as *positive global coupling* (PGC). This situation can be intuitively explained as follows. Suppose c_i increases at some location, for instance due to a fluctuation, then the average $<c_i>$ will also slightly increase accordingly. Simultaneously to these changes, the PGC comes into play and acts towards an increase of c_i wherever it is smaller than the average $<c_i>$, and equivalently, a decrease of c_i in regions in which it is greater than the average $<c_i>$. *Mutatis mutandis*, when $\alpha < 0$, the system experiences a *negative global coupling* (NGC) that tends to enhance spatial perturbations and is often referred to as a desynchronizing coupling.

It is known that sufficiently far from equilibrium highly ordered structures can degenerate into a spatiotemporal chaotic or turbulent regime, in analogy to fluid dynamics [56]. The most famous example is probably the state of flowing fluids beyond the laminar threshold defined by the Reynolds number[2] [57, 58]. In the frame of fluid dynamics turbulence is usually referred to as *strong turbulence* [49] and characterized by the coexistence of fluctuations and macroscopic space-time structures [59]. Far from equilibrium reacting systems can also undergo a transition to a state of spatiotemporal chaos or chemical turbulence characterized by the presence of a considerable large number of uncorrelated spatial domains [49, 60].

Near a (supercritical) Hopf bifurcation, spatiotemporal phenomena in RD systems are usually described by the so-called *complex Ginzburg-Landau equation* (CGLE) [48-52, 61]. The CGLE describes the emergence of self-organized spatiotemporal phenomena such as different types of propagating waves and spatiotemporal chaos or turbulence. The instability underlying the transition from uniform to spatially unstable oscillations is referred to as the *Benjamin-Feir (BF)* instability [48, 51, 60, 62]. Beyond the BF boundary, the phase dynamics equation describing the collective behavior of the diffusively coupled individual oscillators has a negative diffusion coefficient, and irregular or chaotic dynamics may develop. Such ‘anti-diffusive’ [61] fluxes increase the phase gradient. Hence, small local fluctuations are amplified instead of damped, as in the case of a positive diffusion coefficient.

[2] The Reynolds number, Re, is a dimensionless control parameter expressing the balance between the nonlinear and dissipative properties of the flow.

Crossing the BF instability, the development of turbulence usually starts via a transition form nearly uniform initial conditions to *phase turbulence*, which is defined as a state in which the amplitude of the local oscillators is relatively constant while its spatial phase fluctuates [48]. When the system is further driven from the BF limit, *amplitude* or *defect*[3] turbulence develops. Here, pattern irregularities are concentrated in localized defects that are nucleated and annihilated at irregular time intervals and locations. Moreover, the coexistence of laminar (ordered) and chaotic (or disordered) regimes characterizes a state referred to as *spatiotemporal intermittency*. Although the initial bifurcations associated to these different regimes have been theoretically investigated in some model systems [49, 63, 64], the classification of experimental systems in these schemes is not trivial [65].

2.2 NONLINEAR PHENOMENA IN ELECTROCHEMICAL SYSTEMS

2.2.1 THE SOLID/LIQUID INTERFACE

Whenever a metal electrode is brought into contact with an electrolyte solution, a reorganization of the charge distribution across the solid/liquid interface arising from the different properties of the two phases takes place. Owing to its high conductivity, the metal phase does not permit the development of an extended internal space-charge region. As a consequence, an ionic redistribution at the liquid side of the interface takes place, and a region with properties different from those of the bulk is set up. This region is known as the *electrical double layer*. It plays a crucial role in almost all electrochemical investigations [66-72]. Figure 2.3 depicts a schematic representation of the microscopic structure of the double layer, as given by the Bockris-Devanathan-Müller model [73].

[3] In the frame of pattern formation, a topological defect or singularity is defined as any departure from the ideal pattern, but the most useful limit is to consider a *localized structure*, embedded in an otherwise ideal pattern [49]. In the phase and amplitude description a defect is usually referred to the case in which the amplitude goes to zero and the phase is not defined.

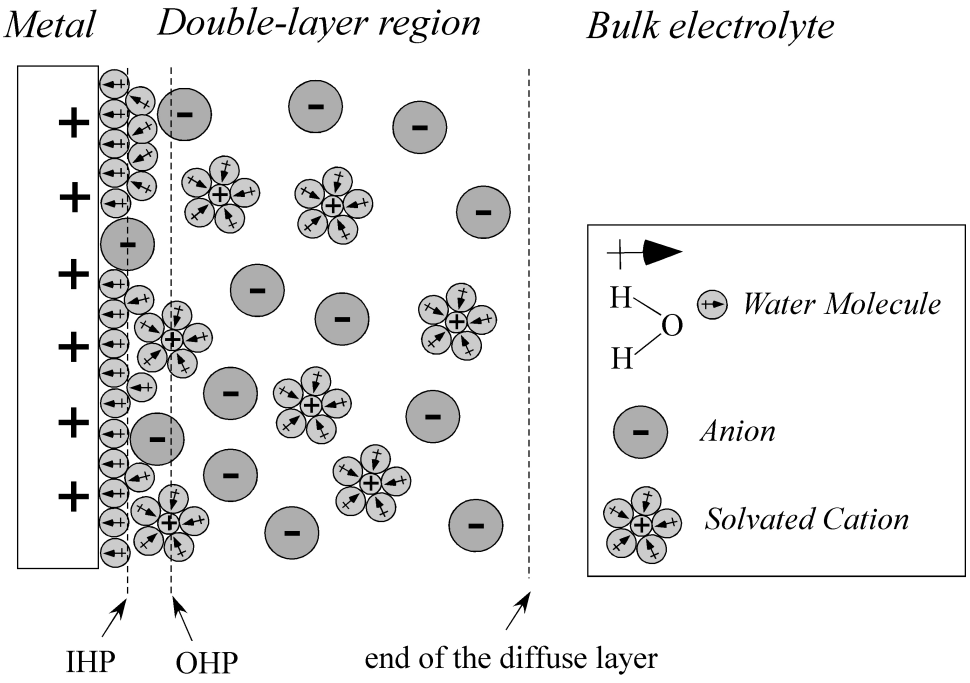

Figure 2.3: Schematic representation of the microscopic structure of the double layer. IHP: inner Helmholtz plane; OHP: outer Helmoltz plane.

The solution side of the double layer can be viewed as comprising several layers. The first layer near the metal surface comprises highly oriented water dipoles and possibly some other species (ions or molecules) that are referred to as being specifically adsorbed. As illustrated in Figure 2.3, due to, short range, van der Waals type interactions, weakly solvated anions have the tendency to undergo *specific adsorption* at the electrode surface even if the metal is negatively charged [70]. The imaginary plane crossing the center of these specific adsorbed anions defines the 'inner Helmholtz plane' (IHP). This two-dimensional region confined between the metal surface and the IHP is usually named the inner or compact layer. The next plane towards the bulk electrolyte is defined by the center of the closest solvated ions (cations in Figure 2.3) and is called 'outer Helmholtz plane' (OHP). The three-dimensional (volumetric) region between the compact layer up to the point where the ionic distribution is no longer disturbed by the presence of the metal is called *diffuse layer*.

Owing to the charge redistribution near the solid/liquid interface, an appreciable potential drop across it is also observed. The potential drop across both the compact and the diffuse layer is called the *double layer potential*, ϕ_{DL}. To probe the potential drop across the interface of interest (at the working electrode, WE) a secondary electrode has to be used. This also implies a charge redistribution around the second interface, and accordingly a potential

drop across it. As a consequence, the absolute electrode potential cannot be measured, and only the difference between the double layer potentials of the WE and RE can be experimentally accessed. φ quantifies this difference and defines the *electrode potential*. In most of the electrochemical systems presenting nonlinear phenomena, the electrode potential, or its equivalent double layer value, ϕ_{DL}, is an essential variable[4]. Moreover, spatial instabilities discussed in this thesis are always associated with potential patterns at the electrode/electrolyte interface. Therefore the interfacial potential, ϕ_{DL}, represents the pivotal variable for the description of self-organization phenomena in this thesis as well as in most electrochemical systems exhibiting dynamic instabilities [27].

2.2.2 THE NEGATIVE DIFFERENTIAL RESISTANCE (NDR)

Most instabilities occurring in electrochemical systems are associated with the existence of a negative slope in the I/ϕ_{DL} curve. The so-called *negative differential resistance* (NDR) is observed, for instance, in an N-shaped stationary I/ϕ_{DL}. Such systems possessing an NDR linked to an N-shaped I/ϕ_{DL} curve are referred to as N-NDR systems. A positive feedback loop, or autocatalytic step, involving ϕ_{DL} may arise due to the interaction between the NDR and the (uncompensated) electrolyte resistance (s.b.). As mentioned above, a positive feedback loop is related to bistability and, at least, one additional loop is necessary for the occurrence of oscillations.

The observation of a current decrease with increasing ϕ_{DL} in N-shaped I/ϕ_{DL} curves is relatively common in electrochemistry [24, 25, 74] and may result from [75]: (a) the decrease of the active electrode area due to an adsorption process that is favored at high values of ϕ_{DL}; (b) the decrease of the electron transfer rate due to the desorption of a catalytic species at high values of ϕ_{DL}; and finally (c) the depletion of reactants concentration at the reaction plane with increasing ϕ_{DL} due to the Frumkin double layer effects [76, 77].

2.2.3 BISTABILITY IN N-NDR SYSTEMS

Figure 2.4 shows a general equivalent circuit of an electrochemical cell. The applied voltage U is divided into two portions: the potential drop across the electrical double layer,

[4] Essential variable means that its time evolution is indispensable for the overall reaction dynamics [54].

ϕ_{DL}, and the ohmic drop through the electrolyte, IR_u, between the RE and the WE. The total cell resistance between the counter electrode (CE) and the WE, R_Ω, is divided into a compensated resistance, R_c, and an uncompensated resistance, R_u, and is thus given by $R_\Omega = R_u + R_c$.

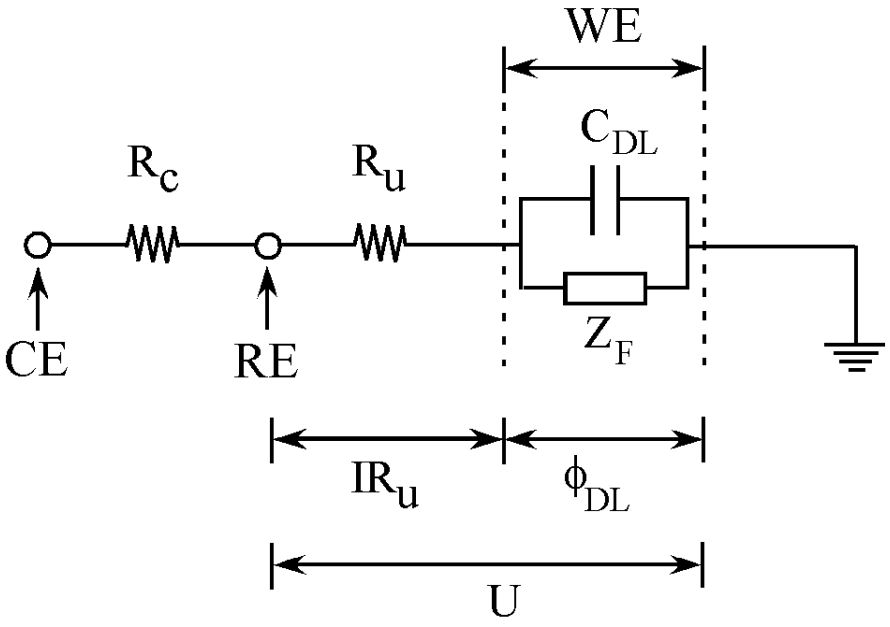

Figure 2.4: General equivalent circuit of an electrochemical cell. $R_{(u)c}$: (un)compensated electrolyte resistance; working (WE), counter (CE) and reference (RE) electrodes; C_{DL}: double layer capacitance; Z_F: general faradaic impedance; U: voltage supplied by the potentiostat; ϕ_{DL}: potential drop across the double layer of the WE. The double layers of the CE and the RE have been omitted for clarity.

The charge balance of the circuit given in Figure 2.4 is obtained by applying Kirchhoff's law and yields

$$C_{DL}\frac{d\phi_{DL}}{dt} + I_F = \frac{U - \phi_{DL}}{R_u}, \qquad (2.3)$$

which means that the sum of the double layer charging and of the reactive or faradaic currents is equal to the current flowing through the electrolyte, which is given by the load line: $(U - \phi_{DL})/R_u$.

Solutions or steady states of equation (2.3) can be obtained graphically. They are given by the intersections between the load line $(U - \phi_{DL})/R_u$ and the I/ϕ_{DL} curve. Figure 2.5 (a) depicts the occurrence of such intersections between an N-shaped I/ϕ_{DL} curve and three

different load lines. Autocatalysis, and thus bistability, in N-NDR systems occurs whenever the uncompensated resistance R_u is larger than the absolute values of the faradaic impedance of the reaction under consideration. In other words, the condition: $R_u > |\partial\phi_{DL}/\partial I|$ should be fulfilled in order to give rise to bistable dynamics. This condition corresponds to the occurrence of a 'folding' in the I/U curve in Figure 2.5 (b).

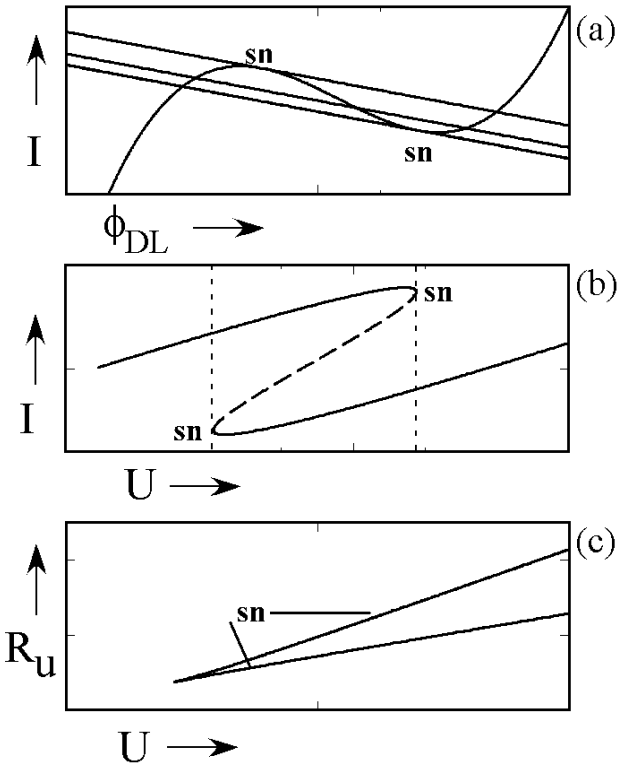

Figure 2.5: (a) N-shaped I/ϕ_{DL} curve and load lines for three different values of the external voltage U. The two outer load lines mark the border of the bistable regime at the specific value of the ohmic resistance. sn: saddle-node bifurcation. (b) Bistable region in an I/U plot referring to the situation shown in (a). (c) Location of the saddle-node (sn) bifurcation (separating monostable and bistable regions) in the R_u/U parameter plane After Krischer [25].

The locations at which a saddle-node bifurcation is expected to take place are denoted by *sn*. As is seen in Figure 2.5 (a), a saddle-node bifurcation can occur when either the uncompensated resistance, R_u, or the applied voltage, U is changed.

Bistability, as shown in Figure 2.1 above, is observed when the applied voltage is varied and it is shown in the I/U curve in Figure 2.5 (b). Varying the applied voltage U, a saddle-node bifurcation occurs when the number of fixed points changes from one to three. Two of the three fixed points are stable; the intermediate one is unstable. Figure 2.5 (c) shows

the bistable region in the U/R_u plane, the borders between the mono- and bistable regions are determined by a saddle-node bifurcation. The bistable region becomes broader for higher U and increasing R_u, independent of the details of the electrochemical reaction.

2.2.4 OSCILLATIONS IN HN-NDR SYSTEMS

In line with the general requirements for oscillations to occur as discussed in section 2.1.2, systems possessing an NDR and hence, at sufficiently high R_u, a positive feedback loop involving ϕ_{DL}, may oscillate in the presence of an additional, negative, feedback loop.

One class of such systems are so-called HN-NDR systems in which a subprocess, at least partially, hides the NDR (so that, 'H' stands for 'hidden'). In general, HN-NDR systems can be viewed as being composed of a subsystem with an N-shaped stationary polarization curve whose NDR is hidden by at least one further slow and potential dependent step of the interfacial kinetics of the total system. Figure 2.6 (a) illustrates the I/ϕ_{DL} curves for an N-NDR (dotted line) and an HN-NDR (full line) system. As is seen in this figure, potential oscillations occur around a region of positive I/ϕ_{DL} slope in the case of an HN-NDR system.

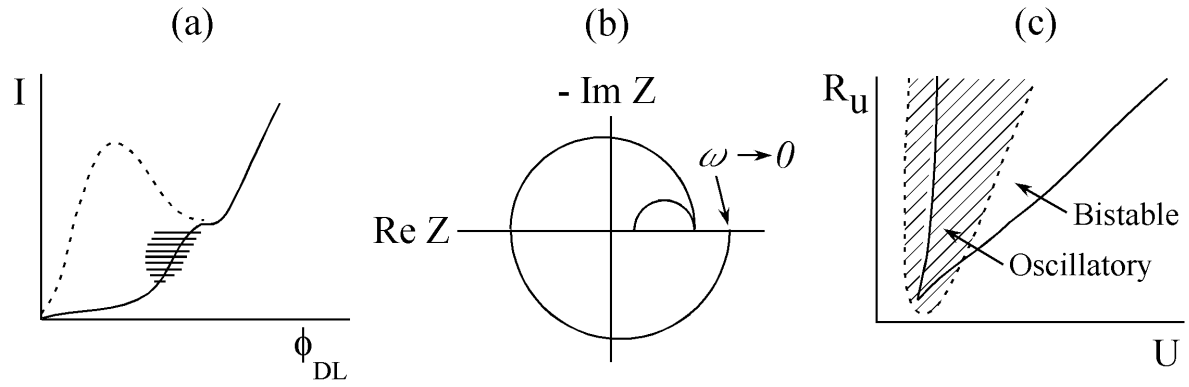

Figure 2.6: (a) Stationary I/ϕ_{DL} curve of H(hidden)N-NDR oscillators (solid line) and N-shaped I/ϕ_{DL} curve of the 'fast subsystem' (dashed line). The oscillations occur for a fixed value of U (potentiostatic conditions) and fixed current (galvanostatic conditions) around a branch with positive slope as indicated by the straight lines for the constant current case. (b) Schematic impedance spectrum for an applied voltage in the oscillatory region of the HN-NDR curve displayed in (a), but under conditions in which the stationary state is stable, i.e., at low R_u. (c) Qualitative locations of bistable and oscillatory regions in the U/R_u parameter plane for HN-NDR oscillators. Note that the oscillatory regions persist up to the limit of infinite R_u, which corresponds to the galvanostatic case.

Figure 2.6 (b) displays the impedance spectrum obtained under conditions in which the stationary state is stable, i.e., for parameter values that are different from the ones of Figure 2.6 (a). Figure 2.6 (b) shows that the slow step mentioned above dominates the faradaic impedance at low perturbation frequencies as in the case of the stationary I/ϕ_{DL} curve depicted in Figure 2.6 (a) (solid line). At higher frequencies, however, the negative impedance of the fast process dominates the impedance behavior. Increasing the uncompensated resistance (or equivalently an external resistance placed in series between the WE and the CE) the entire impedance spectrum shown in Figure 2.6 (b) is shifted to the right side of the diagram. The point at which the circle intercepts the origin of the axis (i.e., Im Z = Re Z = 0) corresponds to the resistance threshold from which on oscillations are observed. In other words, a Hopf bifurcation occurs at this point.

Similarly as done in the bistable case, in Figure 2.6 (c) the locations of bistable and oscillatory regions of an HN-NDR system are depicted in the U/R_u parameter plane. Clearly, HN-NDR oscillators exhibit potential oscillations under galvanostatic conditions and current oscillations under potentiostatic conditions [24, 25].

2.2.5 SPATIALLY EXTENDED REACTION-MIGRATION SYSTEMS

In an electrochemical environment, the equations describing spatiotemporal pattern formation are also composed of a reaction term, i.e. the homogeneous dynamic describing the point-like system, and a part describing the spatial coupling, in a similar way as given in equation (2.1) for RD systems [27]. The primary difference in the equations describing pattern formation in electrochemical systems is that the dominant spatial coupling in this case is through the electric field in the electrolyte. The spatial coupling through the electric field is termed migration coupling, and consequently, the local evolution of the double layer potential is said to be described by *reaction-migration* (RM) rather than reaction-diffusion equations. Since, as explained below, an additive global coupling comes naturally into play in electrochemical systems, the equations describing the local evolution of ϕ_{DL} can be written in general terms as,

$$\frac{\partial \phi_{DL}}{\partial t} = f_i\left(\phi_{DL}, \mu_k, \alpha\right) + \left(\text{migration term}\right) + \alpha\left(\left\langle \phi_{DL} \right\rangle - \phi_{DL}\right), \qquad (2.4)$$

in which the function f_i accounts for the homogeneous dynamics, the migration term for the dominant lateral transport process and the last term refers to the global coupling, respectively.

The fact that the distribution of the electric potential in the electrolyte is governed, to a good approximation, by Laplace's equation, implies that the potential distribution in the electrolyte, and thus also the migration current density at the WE, depends on the potential distribution at the boundaries of the electrolyte. The individual 'elements' composing the electrode surface are coupled among each other by the electric potential distribution in the entire electrolyte, and a change of the double layer potential of one of these individual elements leads to a redistribution of the electric potential in the entire cell. This points to the importance of the cell geometry and the relative arrangement of the electrodes in RM systems. When compared to the diffusion coupling, which is local in nature, migration is considered a non-local coupling (s.b.). Furthermore, theoretical investigations by Mazouz *et al.* [39] showed that the smaller the CE/WE separation, the smaller the lateral extent of the migration coupling. As further discussed below, this opens the perspective of experimentally changing the non-local character of the migration coupling.

The migration coupling just discussed is always present in electrochemical systems. However, there are additional ways by which individual oscillators can be coupled. They arise from the operation mode, i.e., the galvanostatic or the potentiostatic constraint and constitute a global coupling. The coupling induced by the potentiostatic control can be intuitively explained as follows. Suppose a change of ϕ_{DL} at some particular position at the electrode due to some fluctuation, for instance. The electric potential distribution in the entire electrolyte changes because of the strong tendency of the electrolyte to keep the electrolyte electroneutral. The changes of the electric potential in the electrolyte will be most pronounced close to the WE and fades away with increasing distance from it. Hence, if the RE is close to the WE, a local fluctuation of the electrode potential alters the electric potential at the position of the RE noticeably. As a consequence, the actual potential difference between the WE and the RE is different from the set one, and the potentiostat changes the Galvani potential of the WE (or equivalently the Galvani potential of the CE) until actual and set values are identical again. A change of the Galvani potential, however, affects the potential drop across the double layer along the entire electrode/electrolyte interface. Thus, a local change of the double layer potential causes the double layer potential to change everywhere. The coupling induced by the electronic feedback in the potentiostatic operation

mode acts towards desynchronization and tends to enhance the difference in the ϕ_{DL} distribution, favoring the emergence of spatial symmetry breaking [27, 28, 41]. Similarly to the situation illustrated above for RD systems, this coupling is termed *negative global coupling* (NGC). The galvanostatic case will not be investigated in this thesis, and details about its mechanism can be found in ref. [26, 27].

Christoph *et al.* [45, 46, 78] have recently discussed the coupling in electrochemical systems via a coupling function H, which depends only on the system's geometry. The potential distribution in the electrolyte is expressed in terms of the boundary conditions at the electrode with the help of a Green function. The spatial coupling is given in terms of the integral of the coupling function H over the electrode. For an inhomogeneous situation, the coupling function H (x-x') expresses the effect that any location x' has on the dynamics at the position x.

This approach indeed provides a quite intuitive representation of the long-range effects present in electrochemical systems. Figure 2.7 shows the coupling function H for a thin ring electrode of unitary circumference for two different geometries together with the coupling function for the diffusional coupling for comparison (dotted line). The *synchronizing* nature of the migration coupling mentioned above becomes apparent when considering the positive offset in curve *i*, in other words, as H is positive everywhere, the spatial coupling is synchronizing. The *non-local* feature of the migration coupling is also easily seen when comparing curve *i* with the diffusive coupling (dotted line); in contrast to diffusion, migration couples all 'elements' of the electrode with each other, though with different strength.

The next case, curve *ii*, denotes a situation in which the RE is placed between the CE and the WE. Here the nature of the desynchronizing negative global coupling is straightforward. There is a negative offset of the coupling function; adjacent points along the ring remain positively coupled, whereas opposite points are negatively coupled. As stressed earlier, this desynchronizing coupling is termed global since it acts along the entire WE, and the negative shift in the coupling function does not depend on the position.

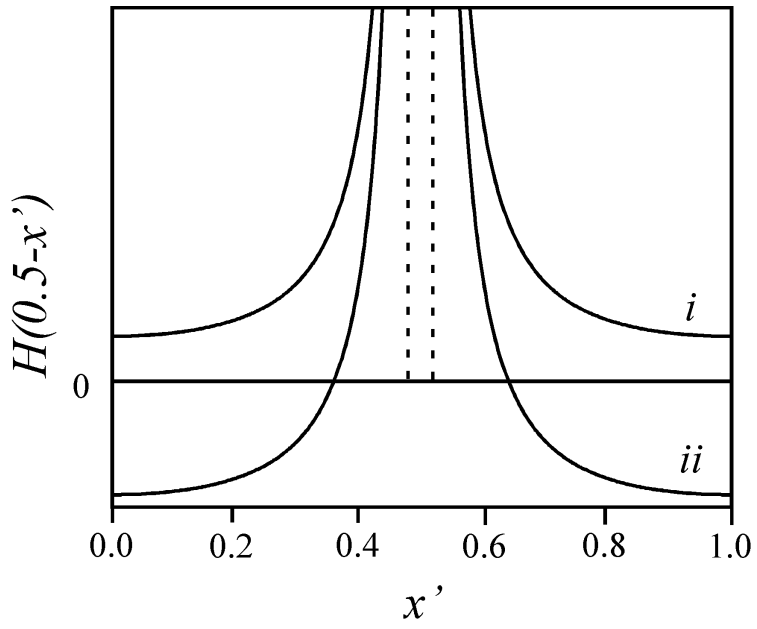

Figure 2.7: Coupling function H as a function of angular coordinate x' for a one-dimensional ring-shaped electrode configuration. Curve *i* corresponds to the situation in which the system is subjected only to migration coupling. In curve *ii* a negative global coupling is superimposed to the system. The dotted line represents the coupling function corresponding to diffusion coupling. After Christoph [46].

Quite recently Krischer and coworkers [79] have reformulated the coefficient entering the evolution equation of the double layer potential in front of the global coupling term. Specifically the coefficient α given in equation (2.4) has been expressed as a function of the compensated and the total cell resistances. The full evolution equation reads,

$$C_{sp}\frac{\partial\phi_{DL}}{\partial t} = -i_F + \frac{U-\phi_{DL}}{AR_\Omega(1+\gamma)} - \sigma\left(\frac{\partial\phi}{\partial z} - \phi\right)\Bigg|_{z=WE} + \frac{1}{AR_\Omega}\frac{\gamma}{1+\gamma}\left(\left\langle\phi_{DL}\right\rangle - \phi_{DL}\right) \qquad (2.5)$$

with

$$\gamma = -\frac{R_c}{R_\Omega}.$$

In this equation C_{sp} is the specific (or per electrode area) double layer capacitance; A is the electrode area; σ the electrolyte conductivity; ϕ the electric potential in the electrolyte; z the coordinate normal to the electrode (pointing into the electrolyte), and z = WE is the

position at the electrolyte end of the double layer of the working electrode; the remaining symbols have already been defined.

The first two terms on the rhs in equation (2.5) represent the homogeneous dynamics, the third term describes the migration coupling [80], and the last term accounts for the global coupling imposed to the system.

From equation (2.5) it becomes apparent that whenever some portion of the electrolyte resistance is compensated, i.e., $R_c \neq 0$, some NGC is induced in the system. The strength of the NGC can then be calculated in terms of R_c and R_Ω, which can easily be measured. As experimentally verified in chapter 6, this reformulation also implies that the way by which the compensation is achieved is irrelevant for the NGC induced. It means that the compensation can be carried out either by using a RE mounted into a Haber-Luggin capillary or by electronic means as in the case of an external resistor with a *negative impedance* characteristics.

2.3 THE HYDROGEN (ELECTRO)OXIDATION REACTION (HOR)

In this section the Hydrogen (electro) Oxidation Reaction (HOR) is reviewed. First the bistable $Pt|H_2SO_4|H_2$, system, which possess an N-shaped polarization curve is discussed. Nonlinear phenomena occurring in this system are discussed in chapter 4. After addition of some electrosorbing ions, such as Cl^- and Cu^{2+}, the N-NDR system is turned into an HN-NDR one. This system exhibits oscillations in wide parameter ranges. It serves as a prototype system in the studies on spatial pattern formation in oscillatory electrochemical systems discussed in chapters 5-8. The mechanism causing oscillations in the $Pt|H_2SO_4$, Cl^-,$Cu^{2+}|H_2$ system is discussed in section 2.3.2.

2.3.1 THE BISTABLE $Pt|H_2SO_4|H_2$ SYSTEM

The well known (see, for instance, ref. [81]), cyclic voltammogram of a platinum electrode in aqueous sulfuric acid electrolyte solution is reproduced in Figure 2.8 (a). According to the applied voltage, the following regions can be identified: (a) the hydrogen adsorption/desorption region between 0 and 0.3 V; the size and shape of the peaks in this region strongly depends on the electrolyte and on the pretreatment of the electrode; (b) the

double layer region between 0.4 and 0.75 V; (c) the oxide formation region which starts in the positive scan at ca. 0.75 V. The oxide reduction takes place at less positive values (ca. 0.71 V in Figure 2.8 (a)) in the backward scan; and (d) the oxygen evolution reaction starting at about 1.45 V. As clearly seen in Figure 2.8 (a), the oxidation process occurs in a very broad potential range, whereas the oxide reduction gives rise to a one much sharper peak. The position of the current peak during the reduction process depends on the extent of the oxidation of the surface. It is shifted towards less positive potentials proportionally to the amount of the oxide formed. The hysteresis observed in the platinum oxidation/reduction reactions [82] is seen even when only a very low amount of oxide is formed, and it is caused by the place exchange processes as will be discussed below.

Figure 2.8 (b) shows the voltammetric signature of the HOR in the $Pt|H_2SO_4|H_2$ system under identical conditions as given in plate (a) but now in the presence of H_2, which is continuously bubbled through the electrochemical cell. In the potential region up to about 0.70 V the main difference between the two CVs is the positive offset current of about 380 μA due to the HOR. From ca. 0.75 V on, the current decreases as the potential increases. Thus an NDR region forms as clearly seen in Figure 2.8 (b). This NDR mediates the transition between an active (high current) and a passive (low current) state. The NDR is caused by the platinum oxide formation which blocks the platinum surface sites leading to a current decrease. The NDR in this N-NDR system can lead to bistability and complex voltammetric responses in low conductivity electrolyte as further discussed in chapter 4.

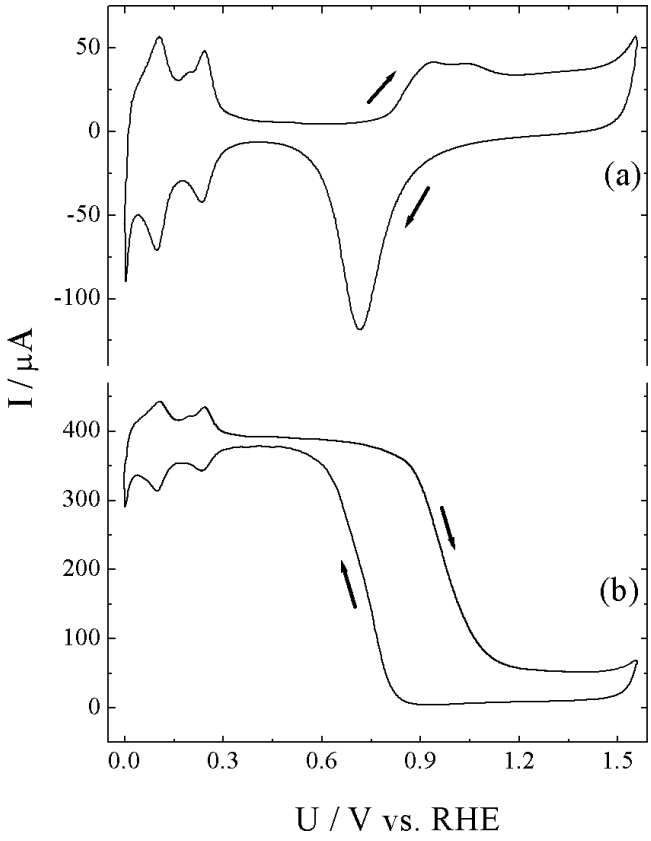

Figure 2.8: Cyclic voltammogram (0.10 Vs^{-1}) of a rotating platinum disk electrode (rotation rate = 20 Hz) in 0.5 M H_2SO_4, (a) saturated with N_2, and (b) saturated with H_2.

The steps underlying the voltammetric response displayed in Figure 2.8 (b) are as follows [83-85]: (i) diffusion of H_2 from the bulk electrolyte to the electrode surface, (ii) dissociative adsorption of surface H_2 onto bare Pt sites, and (iii) electrochemical oxidation of adsorbed hydrogen atoms accompanied by hydration,

$$H_2^{bulk} \rightarrow H_2^{surface}, \qquad \text{(i)}$$

$$2Pt + H_2^{surface} \rightarrow 2Pt - H, \qquad \text{(ii)}$$

$$Pt - H + H_2O \rightarrow H_3O^+ + e^- + Pt. \qquad \text{(iii)}$$

Steps (ii) and (iii) are denoted as Tafel and Volmer steps, respectively, and this mechanism is usually referred to as Volmer-Tafel mechanism [85, 86]. In an electrolyte with high conductivity the electron transfer step (iii) dominates the current only up to about 0.05 V and manifests itself in a steep current increase. As apparent in Figure 2.8 (b), the mass transport

step (i) is rate determining over a wide potential region and, due to the negligible hydrogen dissociation rate (step (ii)) on an oxide covered platinum surface, a current decrease starting at ca. 0.75 V is observed as mentioned above.

The mechanism of platinum oxidation has been recently revised based on electrogravimmetry measurements with an Electrochemical Quartz Crystal Nanobalance, EQCN [87, 88]. In contrary to earlier beliefs (see [89] and references therein), these studies revealed that there is a continuous increase of mass accompanying the oxidation of the platinum surface in the potential range between 0.85 and 1.4 V (vs. RHE) [87, 88]. The main implication of this work is that the two steps scheme,

$$Pt + H_2O \rightarrow Pt - OH + H^+ + e^-$$

followed by,

$$Pt - OH \rightarrow Pt - O + H^+ + e^-$$

is not applicable. Instead, when the oxidation level reaches the value corresponding to one electron per platinum atom (i.e., a charge of 210 μC cm^{-2}) the surface is half covered by O species, rather than by a full monolayer of OH [90]. A similar argument invoking the initial participation of two electrons during the platinum surface oxidation has also been used by Harrington [91].

Thus, the platinum oxide formation proceeds through the discharge of water molecules thereby directly forming PtO [87, 88],

$$Pt + H_2O \rightarrow Pt - O + 2H^+ + 2e^-, \qquad \text{(iv)}$$

the oxide formation may subsequently undergo a place exchange step,

$$Pt - O \rightarrow O - Pt\,. \qquad \text{(v)}$$

As recently pointed out by Conway [92], this result has an important implication on electrocatalytic oxidation mechanisms [93, 94] since at potentials as high as 1.1 V, there are still oxygen free platinum surface sites available which may allow adsorption of reacting species and of anions such as HSO_4^- and Cl^-.

An important point concerning the platinum electrochemistry is the roughening process accompanying the oxide reduction. Phenomenologically, the roughening results from the stripping of subsurface 'O' species which form in the place exchange step [82, 89, 90, 92, 95-100]. The initially deposited oxide is metastable state and undergoes an irreversible transformation to a thin, almost two-dimensional surface oxide phase which is then reduced at less positive potentials than it is formed. The place exchange process leading to the formation of the oxide film is also responsible for the hysteretic effect observed during the oxidation and reduction processes of thin surface oxides on metals [101].

The fact that the processes of oxidation and reduction of platinum can modify the structure of the surface has been recognized a long time ago [102-106]. Although the detailed evolution of the surface structure with, for example, repeated voltammetric cycling, is a very complicated phenomenon and depends on several accompanying processes, it is well known that the platinum oxide reduction enhances the electrode activity by increasing its roughness. In this aspect, it is worth to point out that issues related to this enhancement of the platinum electrode activity, or *electrode activation*, caused by the oxide reduction have been extensively investigated by Burke and coworkers [107-111]. The reason of this surface roughening after the oxide reduction is related to the 'post electrochemical' place exchange process discussed above. Since during the place exchange the platinum atoms move out of their metallic lattice positions driven by the electrochemical potential gradient across the metal/electrolyte interface (which is changed by an imposed bias), it is intuitive to expect that just after oxide reduction the surface possesses a high disorder. In this aspect, morphological changes promoted by the place exchange process have been extensively studied by several groups using many different techniques [89, 112-118].

The scheme in Figure 2.9 summarizes the present discussion. As stressed before, the platinum surface oxidation occurs directly to Pt–O (step *(1)* in Figure 2.9), and the extent of this oxidation is denoted by x. In other words, x is the ratio between oxygen and platinum atoms. After the oxidation process $Pt–O_x$ species can be reversibly reduced back to Pt (step *(1')*) if the oxidation proceeds up to ca. 15 % of the charge of one electron per platinum atom (i.e., 210 μCcm^{-2}), or equivalently $x = 0.07$. For higher charges, however, step *(2)* comes into play, and concomitantly to the platinum oxidation place exchange takes place.

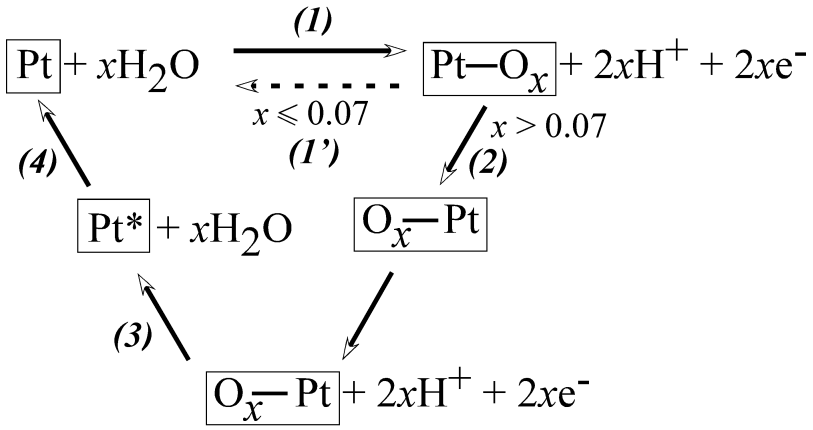

Figure 2.9: Schematic overview of the platinum oxidation/reduction electrochemistry.

The relaxation of a rough to a smooth surface (Pt* to Pt, step *(4)* in Figure 2.9) has also been reported in the literature. Using a somewhat different interpretation at that time, Hoare in his 1982 paper entitled "On the Interaction of Oxygen with Platinum" [119] provides a clear example of the relaxation of a rough platinum surface. In particular, (see Figure 12 in ref. [119]), the platinum electrode was cycled a few times between 0 and 1.5 V (vs. RHE), and then the potential window was restricted to values between 0 and 0.5 V (vs. RHE). Subsequent cycles in this potential region exhibit a continuous decrease of the current in the upd hydrogen peaks and therefore in the real electrode area. After complete surface relaxation into its flattest state, a stationary voltammetric response was reestablished. Very interestingly, after reopening the potential window, i.e., cycling again between 0 and 1.5 V (vs. RHE), only about three cycles were sufficient to recover the previous voltammetric response with the original higher charge in the hydrogen region, and obviously also with the same electrode area as the one observed before cycling in the restricted potential region. Tremiliosi-Filho *et al.* [118] have discussed several changes in the surface roughness as a function of the oxidative treatment of the platinum electrode. For example, they observed an increase of more than three times in surface roughness compared to that of the electrochemically annealed surface when keeping the electrode at 2 V for 48 hours. Furthermore, it was found that the total charge passed, rather than the upper potential limit or number of cycles in voltammetric treatment determines the extent of roughening. The key point concerning the relaxation of the rough surface is that, independent of the oxidizing conditions, the platinum surface always relaxes back to within 5 % of its original real surface area after standard treatment, i.e. electrochemical annealing.

2.3.2 THE OSCILLATORY $Pt|H_2SO_4,Cl^-,Cu^{2+}|H_2$ SYSTEM

In this section it is shown how the bistable $Pt|H_2SO_4|H_2$ system may display oscillations after addition of some electrosorbing species.

Oscillatory dynamics in the HOR in the presence of poisons is a known phenomenon for a long time [120-123] and has been extensively studied both experimentally and theoretically in Krischer's group [53, 124-128]. After these studies it became clear that the mechanism underlying oscillations results from an overlap between the adsorption isotherms of cations and anions which compete for free sites on the metal surface and reduce the rate of H_2 oxidation [126-128]. The electrosorbing species used throughout this work were $Cl^-$and Cu^{2+}, and the whole system is referred to as the oscillatory $Pt|H_2SO_4,Cl^-,Cu^{2+}|H_2$ system.

The effect of successive addition of Cl^- and Cu^{2+} on the HOR is illustrated in Figure 2.10. The solid curve in Figure 2.10 (a) depicts the HOR in the absence of Cl^- and Cu^{2+}. The very steep current increase between 0 and 0.05 V, in which the electron transfer step is rate determining as discussed above, and the subsequent mass transport region characterized by a current plateau in a wide voltage window can be clearly seen. The dashed line in Figure 2.10 (a) illustrates the effect of addition of Cl^-. In this case the I/U curve remains nearly identical to the one obtained in the absence of halide ions (solid line) except from the fact that the adsorption of Cl^- causes a slight current decrease in the mass transport limited region. Hence, Cl^- adsorption causes an NDR, though its slope is small. Addition of Cu^{2+} ions (dotted curve in Figure 2.10 (a)) has an inhibitory effect on the HOR in a potential window corresponding to copper deposition. This inhibitory effect is reflected in the negligible HOR current observed for $U < 0.55$ V (dotted line in Figure 2.10 (a)). At this potential, copper desorption sets in and the current increases. Important in the present context is the fact that the NDR caused by Cl^- is partially hidden by deposited copper, and a positive I/U slope is observed during the copper stripping. Finally, after the copper has been completely stripped from the electrode surface, the current attains again the values corresponding to the ones observed in the $Pt|H_2SO_4,Cl^-|H_2$ subsystem (dashed line in Figure 2.10 (a)).

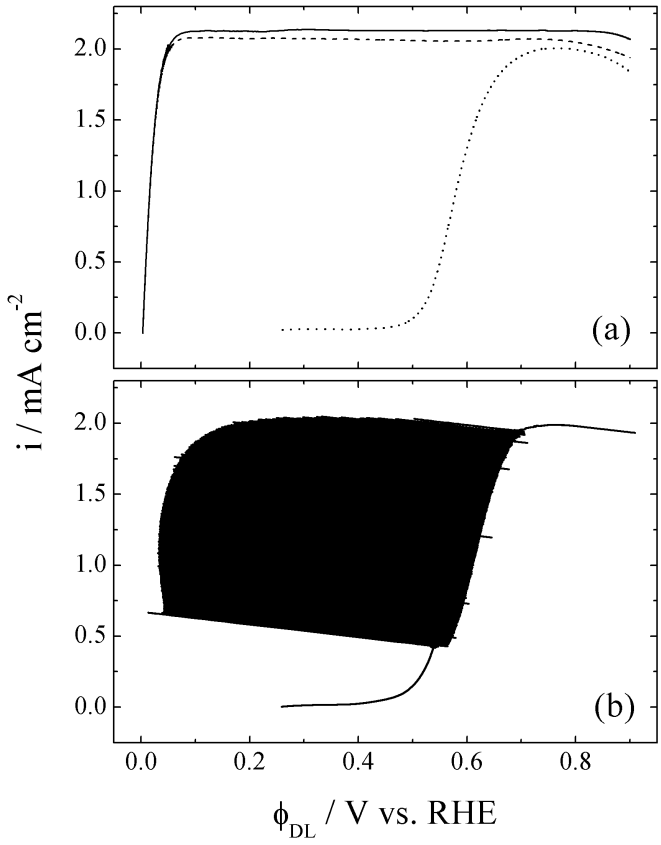

Figure 2.10: (a) i/ϕ_{DL} characteristics of the HOR in 0.1 M H_2SO_4 (solid line), 0.1 M H_2SO_4 and 1 mM HCl (dashed line), and 1 mM H_2SO_4, 1 mM HCl and 0.025 mM $CuSO_4$ (dotted line). (b) i/ϕ_{DL} curve for the same solution as in (a) (dotted line) but with an external resistor in series to the WE such that R_t (= R_{ext} + R_Ω), was 11 kΩ. The data in both plots were obtained after subtracting IR_t from the applied voltage U ($\phi_{DL} = U - iAR_t = U - IR_t$). In these experiments a rotating (ω = 20 Hz) platinum disk was used as WE and the scan rate was 0.002 Vs^{-1}. In all experiments H_2 was continuously bubbled through the solution. For details see ref. [53].

It was discussed in section 2.2.4 that in an HN-NDR system oscillations are expected from a certain critical value of the uncompensated resistance on. The i/ϕ_{DL} curve shown in Figure 2.10 (b) was obtained when an external resistance was inserted in series between the WE and the potentiostat, whereby the sum of this resistance and the uncompensated one amount to 11 kΩ. As clearly seen, potential oscillations are observed in a region of the i/ϕ_{DL} curve which has a positive slope (cf. dotted curve in Figure 2.10 (a)). Moreover, the potential oscillates between the i/ϕ_{DL} curves obtained with and without copper.

The two feedback loops underlying the oscillatory dynamics in the $Pt|H_2SO_4,Cl^-,Cu^{2+}|H_2$ system are shown in Figure 2.11 and can be rationalized as follows. The positive

feedback loop assures that an initial increase in ϕ_{DL} leads to its further increase owing to fast Cl^- adsorption that inhibits the hydrogen current and thus promotes a further increase in ϕ_{DL} (since under potential control $U = \phi_{DL} + IR_u$). In the negative feedback loop, in contrast, an increase in ϕ_{DL} is suppressed because at more positive potentials Cu desorbs, increasing the current and, owing to the potentiostatic constraint, the potential is shifted towards more negative values.

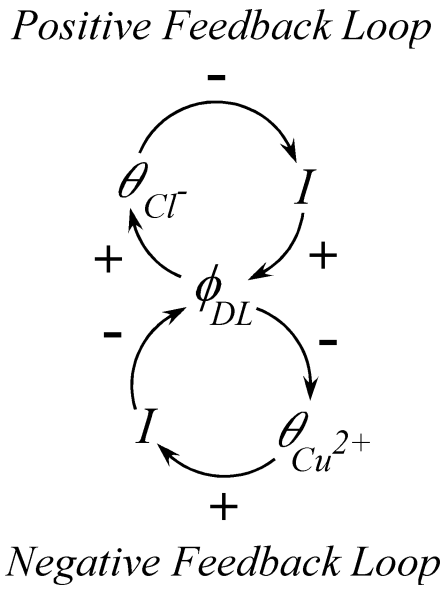

Figure 2.11: Schematics of the two feedback loops present in the HN-NDR $Pt|H_2SO_4,Cl^-,Cu^{2+}|H_2$ system.

Plenge *et al.* [53, 129] have developed a homogeneous model consisting of a set of four ordinary differential equations which was found to capture the main dynamical features of the $Pt|H_2SO_4,Cl^-,Cu^{2+}|H_2$ system. It overcame the key discrepancies between previous models and experiments [126-128]. A very important point included in the model was the interaction between adsorbed Cl^- and Cu^{2+}, such that the anion adsorption is enhanced in the presence of copper at the electrode. Indeed, the inclusion of a term accounting for this interaction was found to be a necessary condition for the agreement between experimental and simulated data [53, 129].

An example of the superior agreement between simulations and experiments is given in Figure 2.12. In plate (a) the calculated (solid line) and experimentally (dots) obtained locations of the Hopf bifurcations are shown. Figure 2.12 (b) shows an experimental i/U

curve obtained with a slow scan rate. From such curves the bifurcation points depicted in plate (a) were obtained.

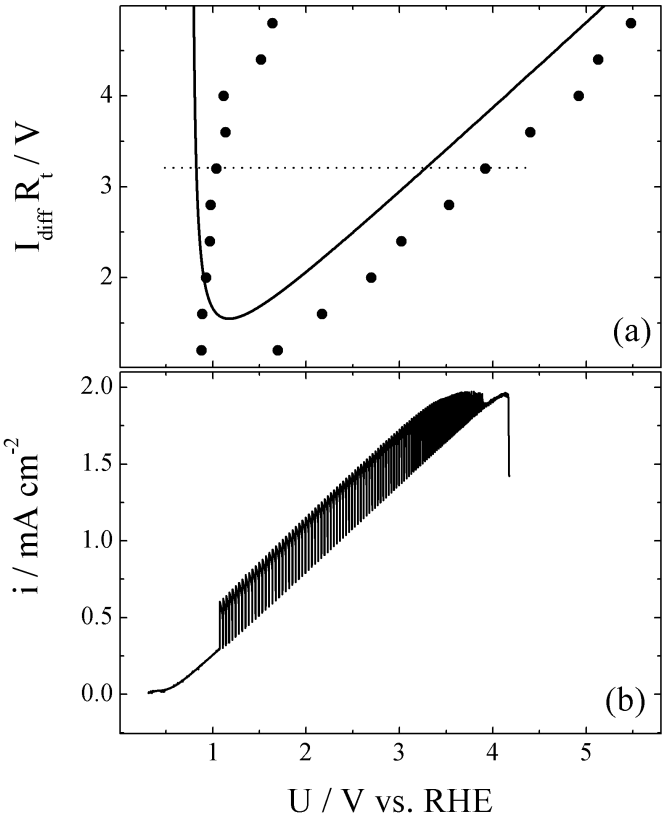

Figure 2.12: (a) Oscillatory region in the $I_{diff}R_t/U$ plane. Solid line: calculated onset of Hopf bifurcation; points: the experimentally observed locations of Hopf bifurcations for ten different values of the external series resistance. The point size in (a) indicates also the error bars. (b) Example of an anodic scan at 0.002 Vs^{-1} displaying the oscillatory region indicated in the dashed line in (a) for R_t = 7 kΩ. Experimental details as in Figure 2.10 (b).

The $Pt|H_2SO_4,Cl^-,Cu^{2+}|H_2$ system serves as a prototypical HN-NDR system. In fact, results obtained for this system can be used to further understand other mechanistically equivalent systems. One interesting example of such a similar system would be the hydrogen oxidation in the presence of small amounts of CO [130, 131]. This system can be compared to the $Pt|H_2SO_4,Cl^-,Cu^{2+}|H_2$ system whereby CO takes the role of Cu adsorbing at less positive potential values and halide becomes unnecessary, since the adsorption of oxygenated species can play the role of competitively adsorbing with CO in a specific potential range. Thus, it should be possible to deduce a lot about the dynamic behavior in the (from the dynamic point of view much less studied) $Pt|H_2SO_4|H_2,CO$ system from the knowledge about instabilities in the $Pt|H_2SO_4,Cl^-,Cu^{2+}|H_2$ model system [132].

2.4 PATTERN CHARACTERIZATION: THE KARHUNEN-LOÈVE DECOMPOSITION

The observed one-dimensional (1-D) spatiotemporal patterns were characterized by the Proper Orthogonal Decomposition (POD) or Karhunen-Loève Decomposition (KLD). In this method the spatiotemporal data set is decomposed into a set of time-*independent* spatial structures and their corresponding time-*dependent* scalar amplitudes. The KLD method is often used to analyze experimental data (typically patterns in space and time) aiming at extracting dominant features ('coherent structures'). In the context of spatiotemporal pattern-forming chemical experiments, it has been successfully used in several systems such as catalytic oxidation of hydrogen on nickel [133], CO oxidation on Rh black/SiO_2 [134] and Pt [135], and iron electrodissolution [136], for example.

In chapters 5 and 7 the measured interfacial potential along the ring-shaped WE, $U_{PP}(x,t)$ was normalized in two different ways before employing the KLD. First, in order to identify spatial structures in the presence of homogeneous oscillations, the spatial average at each instant in time is subtracted from the data $U_{PP}(x,t)$,

$$u_{PP}(x,t) = U_{PP}(x,t) - \frac{1}{L}\int_{L=0}^{2\pi} U_{PP}(x,t)dx = U_{PP}(x,t) - \langle U_{PP}(t)\rangle_x \qquad (2.6)$$

where L is circumference of the WE.

In the second case, the average of the homogeneous offset was subtracted, i.e.,

$$\tilde{U}_{PP}(x,t) = U_{PP}(x,t) - \frac{1}{L}\frac{1}{T}\int_{t=0}^{T}\int_{L=0}^{2\pi} U_{PP}(x,t)dxdt \qquad (2.7)$$

where T is total time of the time series. Either the data obtained as in (2.6) or as in (2.7) were used in the KLD. The data normalized in according to (2.6) are referred to as the inhomogeneous part of the interfacial potential in the following chapters. The 'full' data normalized with the procedure given in (2.7) will be simply referred to as the interfacial potential.

Taking the spatiotemporal set of data $u_{PP}(x,t)$ given in (2.6), the elements r_{ij} of the correlation matrix R can be defined as,

$$r_{ij} = \frac{1}{M}\sum_{m=1}^{M}\left[u_{PP}(x_i, t_m)u_{PP}(x_j, t_m)\right] \quad i, j = 1,\ldots, N. \qquad (2.8)$$

Where N stands for the number of discrete points in space and M for the instants in time.

The eigenvectors χ_i of the matrix R are linearly independent and form a complete orthonormal set. They represent the dominant spatial structures (s.b.). The corresponding eigenvalue λ_i represents the significance with which the eigenvector (or mode) χ_i contributes to the overall spatiotemporal pattern and is maximized in the way that:

$$\lambda_i = \left\langle (u_{PP}, \chi_i)^2 \right\rangle, \qquad (2.9)$$

in which the parentheses account for the inner product, whereas the angle brackets stand for the average.

The set $u_{PP}(x,t)$ can be conveniently represented in terms of the eigenvectors χ_i:

$$u_{PP}(x,t) = \sum_{j=1}^{M} C_j(t)\chi_j(x), \qquad (2.10)$$

in which the temporal uncorrelated coefficients C_i are obtained by projecting the data onto the eigenvectors:

$$C_i(t) = (\chi_j(x), u_{PP}(x,t)). \qquad (2.11)$$

This procedure provides an objective method for determining the spatial structures with the highest 'energy'. In quantitative terms, one seeks the functions $\chi_i(x)$ with the largest amplitude $C_i(t) = (u_{PP}(x,t), \chi_i(x))$ in a mean square sense. Among all linear decompositions, the KLD can be considered the most efficient for modeling or reconstructing the signal $u_{PP}(x,t)$, in the sense of capturing the dominant components of an infinite-dimensional process with a finite number of 'modes' (i.e. the functions $\chi_i(x)$) [137].

Finally, it should be mentioned that the KLD analysis reported in this thesis was carried out in cooperation with Dr. Antoine Bonnefont whose help is strongly acknowledged.